scientific reports

Check for updates

OPEN

Gingipain regulates isoform switches of PD-L1 in macrophages infected with *Porphyromonas gingivalis*

Yilin Zheng[1,5], Ziyi Wang[2,5], Yao Weng[1], Heriati Sitosari[1,3], Yuhan He[1], Xiu Zhang[1], Noriko Shiotsu[4], Yoko Fukuhara[1], Mika Ikegame[1] & Hirohiko Okamura[1]✉

Periodontal pathogen *Porphyromonas gingivalis* (*P. gingivalis*) is believed to possess immune evasion capabilities, but it remains unclear whether this immune evasion is related to host gene alternative splicing (AS). In this study, RNA-sequencing revealed significant changes in both AS landscape and transcriptomic profile of macrophages following *P. gingivalis* infection with/without knockout of gingipain (a unique toxic protease of *P. gingivalis*). *P. gingivalis* infection increased the PD-L1 transcripts expression and selectively upregulated a specific coding isoform that more effectively binds to PD-1 on T cells, thereby inhibiting immune function. Biological experiments also detected AS switch of PD-L1 in *P. gingivalis*-infected or gingipain-treated macrophages. AlphaFold 3 predictions indicated that the protein docking compatibility between PD-1 and *P. gingivalis*-upregulated PD-L1 isoform was over 80% higher than another coding isoform. These findings suggest that *P. gingivalis* employs gingipain to modulate the AS of PD-L1, facilitating immune evasion.

Keywords *Porphyromonas gingivalis*, Gingipain, Macrophage, Alternative splicing, PD-L1, Immune evasion

Porphyromonas gingivalis (*P. gingiavlis* or *Pg*) is considered the primary pathogen responsible for periodontal disease[1]. *P. gingivalis* promotes the development of the disease by producing multiple proteolytic enzymes that degrade periodontal tissues[2]. Among these proteases, gingipains are considered major contributors to the proteolytic activity of *P. gingivalis*[3]. Gingipains, a family of proteases sharing similar structures, include members such as RgpA and RgpB, which cleave arginine residues, and Kgp, which cleaves lysine residues[4]. *P. gingivalis* utilizes gingipains to degrade iron-binding proteins and key extracellular matrix components, such as junctional adhesion molecule 1, thereby disrupting the epithelial barrier and facilitating penetration into subepithelial tissues to invade periodontal structures[5]. Additionally, gingipains cleave T cell surface proteins, including CD4 and CD8, as well as pro-inflammatory cytokines, such as interleukin (IL)-6, IL-8, IL-12, and interferon-gamma. These activities disrupt the host immune response and promote immune evasion[6,7]. However, whether gingipains directly affect host gene transcription and protein translation remains unexplored.

Previously, we found that *P. gingivalis* infection of macrophages leads to histone leakage[8]. Histone modifications are known to affect alternative splicing (AS) of mRNA[9,10]. The capacity to generate various transcripts (gene isoforms) through AS significantly contributes to the complexity of proteome in higher vertebrates. A vast majority of human genes utilize alternative isoforms: around 95% of multi-exon genes exhibit evidence of AS, and about 60% of genes have at least one alternative transcription start site[11]. This splicing diversity plays important biological roles in organisms, including increasing protein functional diversity, regulating gene expression levels, and participating in processes such as cell development and tissue specialization. The changes in AS of the transcriptome in infected macrophages are crucial in regulating the immune response[12]. However, the role of mRNA AS in macrophages infected with *P. gingivalis* has not been elucidated.

[1]Department of Oral Morphology, Graduate School of Medicine, Dentistry and Pharmaceutical Sciences, Okayama University Hospital, Okayama University, 2-5-1 Shikatacho, Kita-ku, Okayama 700-8525, Japan. [2]Department of Molecular Biology and Biochemistry, Graduate School of Medicine, Dentistry and Pharmaceutical Sciences, Okayama University, Okayama 700-8525, Japan. [3]Department of Oral Biology, Faculty of Dentistry, Universitas Gadjah Mada, Yogyakarta 55281, Indonesia. [4]Comprehensive Dental Clinic, Okayama University Hospital, Okayama University, Okayama 700-8525, Japan. [5]Yilin Zheng and Ziyi Wang have contributed equally to this work. ✉email: hiro-okamura@okayama-u.ac.jp

P. gingivalis has been shown to induce the upregulation of the immune checkpoint protein, programmed death ligand 1 (PD-L1), in periodontal tissue cells[13,14]. PD-L1, encoded by the CD274 gene, is the ligand for the co-inhibitory receptor programmed cell death protein 1 (PD-1)[15]. Under physiological conditions, PD-L1 is expressed in various immune-privileged organs. Additionally, many immune-related cells express PD-L1, especially activated T and B lymphocytes, dendritic cells, monocytes, mesenchymal stem cells, and bone marrow-derived mast cells. The interaction of PD-1 with PD-L1 provides immune escape for immune-privileged organs or tumor cells by inhibiting T cell activation and cytokine production. This leads to the attenuation of T cell responses by blocking proliferation, inducing apoptosis, and promoting the differentiation of regulatory T cells[16].

AS in cancer generates neoantigens that can evade immune detection, affecting immunotherapy outcomes. AS in PD-L1 induces resistance to PD-L1 blockade in non-small cell lung cancer[13,14]. PD-L1 protein is a transmembrane glycoprotein with a substantial extracellular region that includes Immunoglobulin-like domains, a hydrophobic transmembrane domain, and a 30-amino acid cytoplasmic tail that does not have canonical signaling motifs[17]. The Immunoglobulin (Ig)-like domains can be divided into two types: one is the Immunoglobulin Variable (IgV)-like domain, and the other is the Immunoglobulin Constant (IgC)-like domain. According to the Ensembl database, two alternative coding transcripts of PD-L1 are encoded by the CD274 gene[15,18]. The longer coding transcript, PD-L1 with IgV-like domain (PD-L1^{IgV+}), contains all exons from 1 to 7 and encodes a 290 amino acid protein (33 kDa). The second transcript, PD-L1 lacking IgV-like domain (PD-L1^{IgV-}), produced by AS, lacks exon 3, resulting in a shorter 160 amino acid isoform without an IgV-like domain. Given that the IgV-like domain is crucial for the interaction of PD-1 with PD-L1 [19,20], therefore, different PD-L1 isoforms may have different effects on inhibiting T cell function. However, the AS of PD-L1 has not been reported in the *P. gingivalis*-infected macrophages.

In this study, we explored the landscape of isoform switches in macrophages infected with *P. gingivalis* using high-throughput RNA sequencing. Our bioinformatics analysis revealed that PD-L1 plays a crucial role in regulating the immune response in macrophages exposed to *P. gingivalis* through gingipain release. We not only identified switches in AS and the transcriptome related to the immune response in *P. gingivalis*-infected macrophages but also validated the AS events of PD-L1 in *P. gingivalis* (with/ without gingipain) -infected and gingipain-treated macrophages through biochemical experiments. These findings suggest a novel mechanism by which *P. gingivalis* may facilitate immune evasion in chronic periodontitis.

Results

Landscape of AS events in *Pg*-inf macrophages with/without gingipain

To investigate whether *P. gingivalis* infection, with or without gingipain, induces different significant AS (Sig. AS) events and patterns in macrophages, human monocytic THP-1 cells were used to establish No-inf, *Pg*-inf, and *ΔKDP*-inf models (Fig. 1A). RNA sequencing was performed on these samples, and the resulting data were analyzed using bioinformatics software, as mentioned in the Methods section. The landscape of gene comparisons, highlighting different Sig. AS events and patterns in the established infection models, is illustrated in Fig. 1B,C. In the pairwise comparisons of genes across the No-inf, *Pg*-inf, and *ΔKDP*-inf groups, we detected different AS events and variation patterns. This finding suggests that *P. gingivalis* infection influences the original AS in macrophages, with gingipains playing a significant role in this process.

AS events of PD-L1 (CD274) were identified following *P. gingivalis* infection through bioinformatics analysis

The Venn diagram illustrates the screening process for genes closely associated with gingipains from previous RNA sequencing data during *P. gingivalis* infection (Fig. 2A). The overlapping section of Set 1 and Set 2 revealed that AS events in 32 genes were associated with gingipains, while Set 3 further identified that AS events in 26 of these 32 genes occurred specifically during the infection process. In the functional enrichment analysis of these 26 overlapping genes, "GO:0050870_positive regulation of T cell activation" was found in the top 20 categories (Fig. 2B). PD-L1 (CD274), as the most significantly upregulated gene, was enriched in this category (Fig. 2C).

To further investigate the specific AS events of PD-L1 after *P. gingivalis* infection, we conducted isoform switch analysis in "No-inf versus *Pg*-inf" (Fig. 2D–F). In this analysis, two types of PD-L1 coding isoforms, PD-L1^{IgV-} and PD-L1^{IgV+} were identified (Fig. 2D). *P. gingivalis* infection resulted in an increase ($p < 0.001$) in PD-L1 gene expression (Fig. 2E) based on the Transcripts Per Million value. However, the isoform usage of PD-L1^{IgV-} decreased ($p < 0.05$) after *P. gingivalis* infection (Fig. 2F). AS events and patterns of PD-L1 can also be identified in the "*Pg*-inf versus No-inf" comparison (Fig. 1B–C) and the predicted relationship between two PD-L1 coding isoforms is shown in Fig. 2G. Therefore, we predict that *P. gingivalis* infection not only upregulated macrophage gene expression of PD-L1 but also specifically upregulated the PD-L1^{IgV+} isoform.

Gingipain-expressing *P. gingivalis* infection preferentially enhanced the expression of PD-L1^{IgV+} in macrophages

To evaluate the effects of gingipain on PD-L1 protein expression in macrophages, Western blot analysis was performed to assess the PD-L1 protein levels in macrophages under previously described infection conditions (Fig. 1A). The results and grayscale analysis of the Western blot analysis is shown in Fig. 3A–B. Compared to No-inf, *Pg*-inf significantly upregulated the expression of PD-L1 in macrophages ($p < 0.01$). There was no statistically significant difference in PD-L1 protein expression between *ΔKDP*-inf and No-inf ($p = 0.4355$). Furthermore, PD-L1 protein expression was significantly decreased in *ΔKDP*-inf compared to *Pg*-inf ($p < 0.01$). These findings suggest that *P. gingivalis* infection enhances PD-L1 expression in macrophage in a gingipain-dependent manner.

Because the PD-L1 antibody recognizes all isoforms of PD-L1 proteins, we performed RT-PCR and RT-qPCR to investigate the AS of PD-L1. We designed a primer spanning Exon 3 (IgV-like domain) and Exon 4

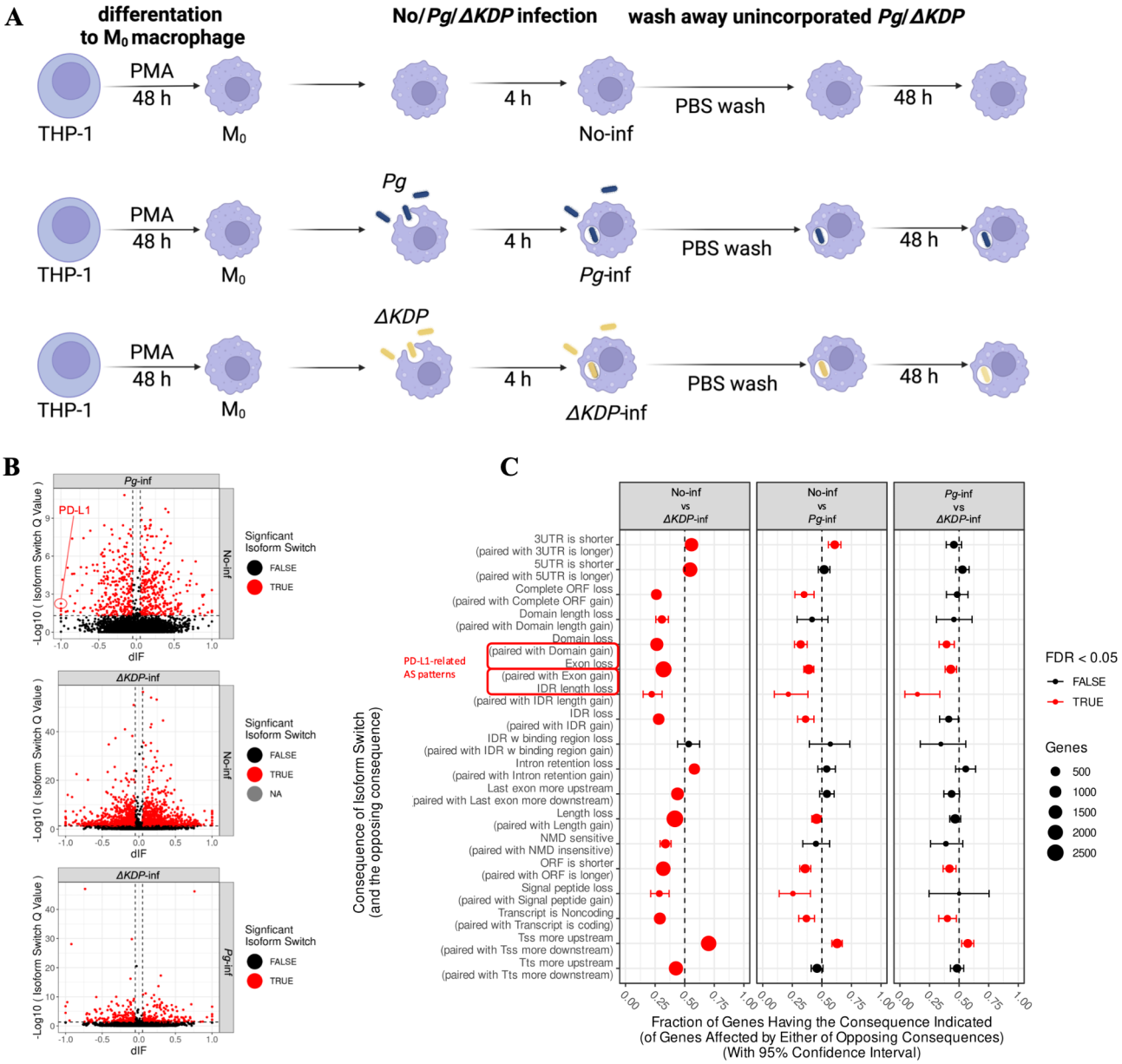

Fig. 1. Landscape of AS events in No-inf, *Pg*-inf, *ΔKDP*-inf macrophages. (**A**) Workflow for establishing of No-inf, *Pg*-inf, and *ΔKDP*-inf macrophages. (**B**) Volcano plots show differential AS events in the comparisons "*Pg*-inf versus No-inf", "*ΔKDP*-inf versus No-inf", and "*Pg*-inf versus *ΔKDP*-inf". Sig. AS events (FDR < 0.05 and |log2Fold Change| > 1) were identified based on differences in isoform fraction (dIF). PD-L1-related AS events can be identified in "*Pg*-inf versus No-inf" with dIF = − 1, $-\text{Log}_{10}$(Isoform switch Q value) = 1.869. (**C**) Differential AS patterns are displayed for the same comparisons in No-inf, *Pg*-inf, and *ΔKDP*-inf macrophages. The size of each dot represents the number of associated genes, with significant changes defined as FDR < 0.05. The AS patterns of PD-L1 can be identified in "Domain loss (Paired with domain gain)" and "Exon loss (Paired with exon gain)". Both (**B**) and (**C**) were analyzed by IsoformSwitchAnalyzeR software.

(IgC-like domain) of PD-L1^{IgV+} isoform (right panel of Fig. 4C). The RT-PCR products of total RNA from No-inf macrophages using this primer are shown in the left panel of Fig. 4C. Three distinct bands were detected, corresponding to the locations of the three reported PD-L1 isoforms in Ensembl. These bands represent CD274-202, PD-L1^{IgV+} isoform (805 bp); CD274-205, Non-coding isoform (632 bp); and CD274-201, PD-L1^{IgV-} isoform (463 bp). These results indicate that multiple isoforms are present in normal macrophages.

To further investigate the AS of PD-L1 in *Pg*-inf and *ΔKDP*-inf macrophages, we designed specific primers targeting the PD-L1^{IgV-} and PD-L1^{IgV+} isoforms for RT-qPCR analysis. The results revealed that the expression of PD-L1^{IgV-} showed a modest increase in *Pg*-inf compared to No-inf ($p < 0.05$), while no significant difference was observed between *Pg*-inf and *ΔKDP*-inf ($p = 0.7990$) (Fig. 4D). In contrast, PD-L1^{IgV+} was significantly upregulated in *Pg*-inf compared to both No-inf ($p < 0.0001$) and *ΔKDP*-inf ($p < 0.0001$), with no significant

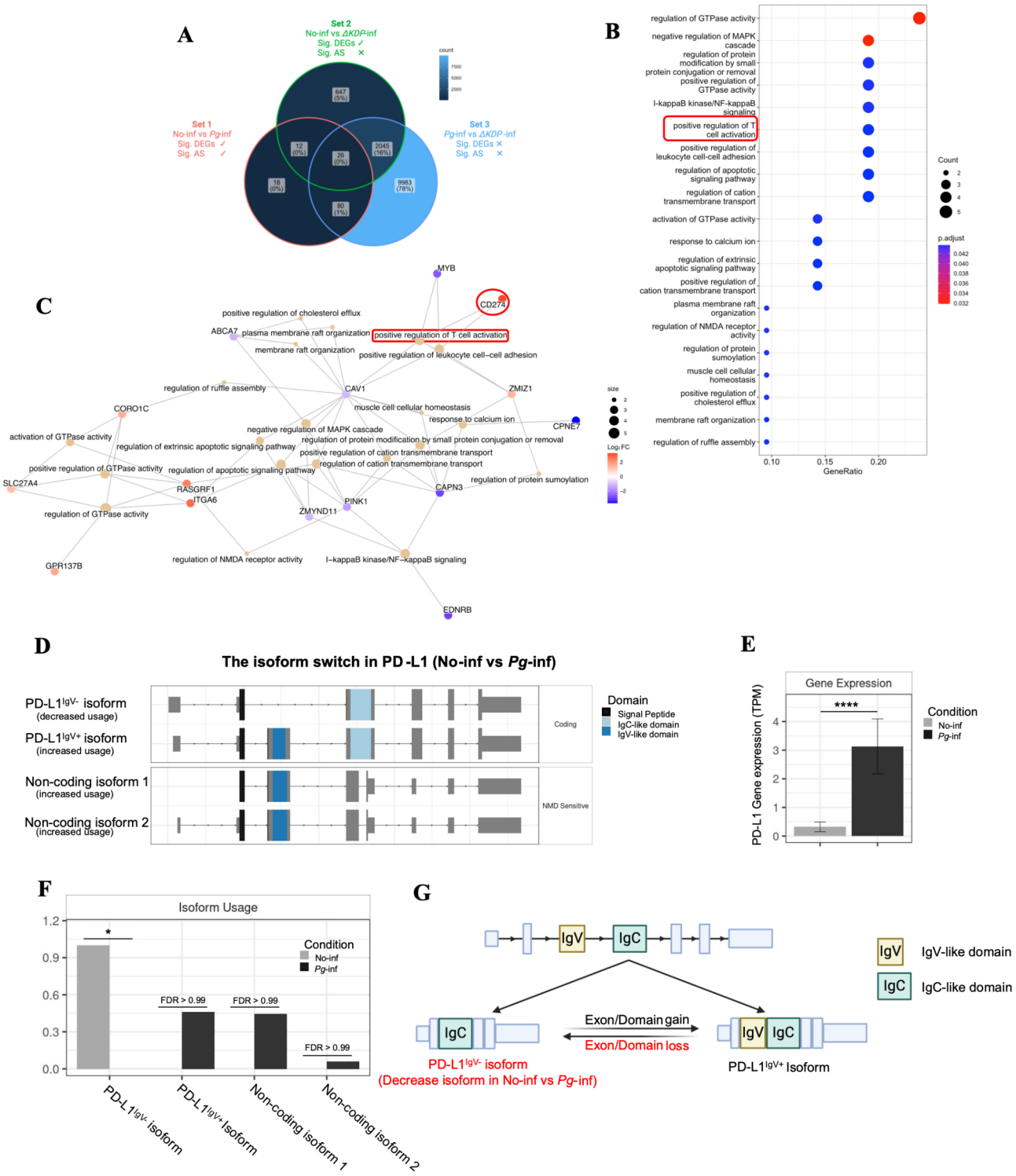

difference between No-inf and *ΔKDP*-inf ($p = 0.5581$) (Fig. 4E). These findings indicate that Gingipain-expressing *P. gingivalis* infection specifically drives the expression of the PD-L1^{IgV+} isoform. We also compared the relative expression levels of PD-L1^{IgV-} and PD-L1^{IgV+} isoforms within each group (No-inf, *Pg*-inf, and *ΔKDP*-inf macrophages) using $2^{-\Delta Ct}$ (Fig. S1A). In the *Pg*-inf macrophages, the relative expression level of PD-L1^{IgV+} was higher than that of PD-L1^{IgV-} ($p < 0.0001$). The exon-inclusion ratio, also known as percent spliced in, is a widely used metric for quantifying AS events[21]. To examine the modulation of PD-L1 AS by gingipain, we utilized the data from Fig. S1A to calculate the PSI within No-inf, *Pg*-inf, and *ΔKDP*-inf macrophages (Fig. 4F). Our analysis revealed that PD-L1^{IgV+} accounted for 95% of the total coding sequence in *Pg*-inf macrophages. In No-inf macrophages, PD-L1^{IgV+} usage was 79%, while in *ΔKDP*-inf macrophages, the usage dropped to 69%. These findings suggest that infection with Gingipain-expressing *P. gingivalis* modulates the AS of PD-L1, favoring the expression of PD-L1^{IgV+} isoform, consistent with our previous RNA sequencing findings.

◀**Fig. 2**. PD-L1 targeted by isoform switch following *P. gingivalis* infection. (**A**) 26 genes were identified as highly relevant to gingipain during *P. gingivalis* infection of macrophages, based on whether they were classified as DEGs ($p < 0.05$ and dIF > 0.05) and/or Sig. AS events with dIF value (FDR < 0.05 and |log2Fold Change| > 1) across Set 1, Set 2, and Set 3. (**B**) The functional enrichment analysis dot plot shows the top 20 related GO Biological Process (BP) terms associated with 26 selected genes in (**A**). Dot size represents the number of associated genes (Count), and *p*.adjust < 0.05. (**C**) The Netplot illustrates the relationships between the 26 selected genes in (**A**) and the top 20 GOBP categories in (**B**). (**D**) Four isoforms of PD-L1 were identified in the "*Pg*-inf versus No-inf" comparison. **(E)** PD-L1 gene expression of with or without *P. gingivalis* infection is shown based on the gene transcripts per million (TPM) values analyzed by DEseq2. (**F**) The isoform usage of PD-L1 under the same condition with (**E**) was analyzed using DEXSeq software. (**G**) Prediction of PD-L1 AS patterns in macrophages infected with *P. gingivalis*. DEGs were detected by DESeq2 software; Differential exon usage (DEU) was detected by DEXSeq software; Analysis of isoform switches was performed by IsoformSwitchAnalyzeR software. *FDR < 0.05, ****FDR < 0.0001.

Recombinant gingipain, RgpA, RgpB and kgp independently upregulated PD-L1^{IgV+} isoform in macrophages

Studies have shown that gingipain knockout weakens *P. gingivalis* activity, reducing its viability[22]. To determine whether the recovery of PD-L1^{IgV+} expression in *ΔKDP*-inf macrophages results from reduced bacterial activity due to gingipain knockout or is directly dependent on gingipain, we treated macrophages with recombinant gingipains (RgpA, RgpB and Kgp) (Fig. 4A). The results showed that, except for RgpA-treated macrophages, which exhibited no significant upregulation of either PD-L1 isoform (RgpA, IgV-: $p = 0.7980$; IgV+: $p = 0.0645$), both RgpB and Kgp-treated macrophages significantly upregulated the relative expression of PD-L1^{IgV-} (RgpB, IgV-: $p < 0.01$; Kgp, IgV-: $p < 0.01$). However, the upregulation of PD-L1^{IgV+} was much more pronounced (RgpB, IgV+: $p < 0.001$; Kgp, IgV+: $p < 0.001$) (Fig. 4B–C). We also compared the relative expression levels of PD-L1^{IgV-} and PD-L1^{IgV+} isoforms within each group (Untreated, RgpA, RgpB and Kgp-treated macrophages) using $2^{-\Delta Ct}$ (Fig. S1B). Except for untreated macrophages, where no significant difference was observed between the expression of PD-L1^{IgV+} and PD-L1^{IgV-} isoforms ($p = 0.1969$), all three types of gingipain-treated macrophages exhibited significantly higher expression of the PD-L1^{IgV+} isoform compared to the PD-L1^{IgV-} isoform (RgpA, $p < 0.01$; RgpB, $p < 0.001$; Kgp, $p < 0.001$). Subsequent PSI calculations based on the results of Fig. S1B also showed that the proportions of PD-L1^{IgV-} and PD-L1^{IgV+} isoforms were significantly altered in all three gingipain-treated groups compared to the untreated group (RgpA, $p < 0.005$; RgpB, $p < 0.005$; Kgp, $p < 0.005$) (Fig. 4D). These results indicate that gingipain treatment not only upregulates the overall PD-L1 expression in macrophages but also selectively increases the proportion of the PD-L1^{IgV+} isoform by modulating AS. This further indicates that the upregulation of PD-L1 and the alteration in its AS induced by *P. gingivalis* infection in macrophages occur in a gingipain-dependent manner.

AlphaFold 3 predictive modeling shows increased binding of PD-L1^{IgV+} to PD-1 compared to PD-L1^{IgV-}

Since no crystal structure of the human PD-L1^{IgV-}-PD-1 complex has been reported in the RCSB PDB database (http://www.rcsb.org), and the available crystal structure of the PD-L1^{IgV+}-PD-1 complex includes only the IgV-like domain, we utilized AlphaFold 3 to predict the binding interactions of PD-L1^{IgV+} and PD-L1^{IgV-} with PD-1. First, we retrieved the reported the crystal structures of human PD-L1 and PD-1 from the RCSB PDB database and generated AlphaFold 3 models (as described in method section). We compared the predicted models with the RCSB PDB structures using PyMOL (Fig. 5A–B) and found RMSD values of 1.344 for PD-L1 and 0.403 for PD-1 when comparing AlphaFold 3 predictions to the RCSB PDB structures. Additionally, we used AlphaFold 3 to predict a protein structure model based on the sequence corresponding to the PDB entry 3BIK (human PD-L1_mouse PD-1) from the RCSB PDB database. The comparison between the predicted structure and the original 3BIK protein structure showed high similarity (RMSD = 1.718) (Fig. S2). These results indicate that the AlphaFold 3-predicted structures of PD-L1 and PD-1, as well as their docking complex, closely resemble the reported RCSB PDB structures (RMSD < 2)[23,24].

Subsequently, we used AlphaFold 3 to predict the PD-L1^{IgV+}-PD-1 and PD-L1^{IgV-}-PD-1 complexes (Fig. 5C) and performed a comparative assessment. The Chain_pair_inter-chain predicted TM-score (iptm) refers to the accuracy of predicted interactions between protein chains, with higher scores indicating more reliable predictions, commonly used in AlphaFold-Multimer analysis[25]. We found that the chain_pair_iptm of PD-L1^{IgV+}-PD-1 was higher ($p < 0.0001$) than PD-L1^{IgV-}-PD-1 (Fig. 5D). This suggests that PD-L1^{IgV+} binds to PD-1 more effectively than PD-L1^{IgV-}. Additionally, this difference in binding is supported by the hydrogen bonds formed between the amino acid residues of the two PD-L1 isoforms and PD-1 (Fig. 5E–F). PD-L1^{IgV+} forms 18 hydrogen bonds with PD-1, while PD-L1^{IgV-} forms only 10 hydrogen bonds with PD-1. These results further confirm that, during *P. gingivalis* infection, the selective upregulation of PD-L1^{IgV+} by gingipain facilitates more effective binding to PD-1.

Discussion

The present study provides evidence that gingipain is involved in AS of PD-L1, an inhibitory immune checkpoint protein, during *P. gingivalis* infection of macrophages. PD-L1, as a well-known transmembrane protein, has been extensively studied in the field of cancer due to its ability to suppress immune responses[26–28]. Some studies have shown that infection with *P. gingivalis* upregulates the expression of PD-L1 in host cells, thereby exacerbating cancer progression[29–31]. In this study, we also found upregulation of PD-L1 in *Pg*-inf macrophages (Fig. 3A–B).

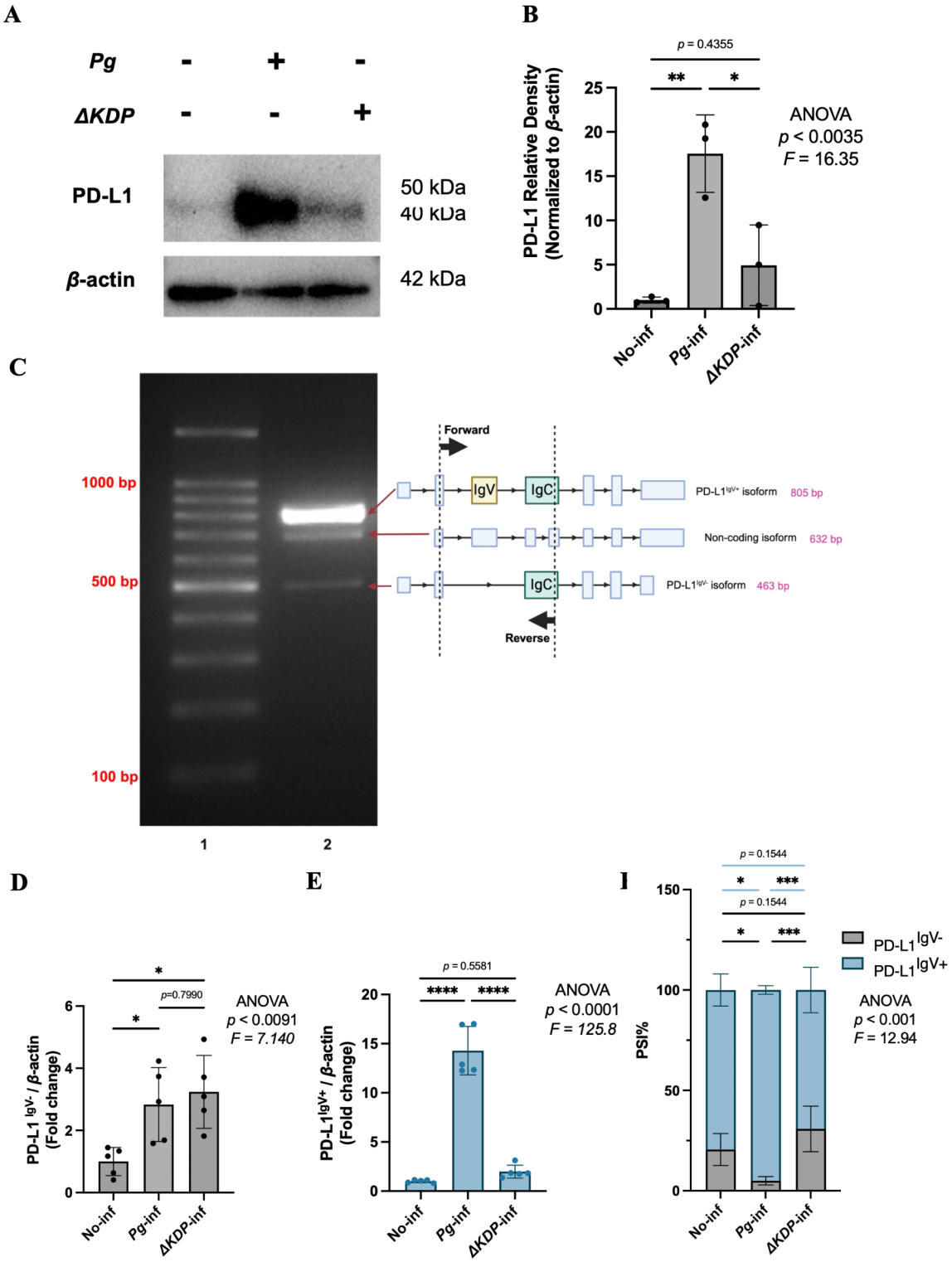

We further showed that *P. gingivalis* not only upregulates the overall expression of PD-L1 through gingipain but also regulates the AS of PD-L1, selectively increasing the PD-L1^{IgV+} isoform (Figs. 3D–F and 4B–D). Evidence indicates that the IgV-like domain of PD-L1 is the primary region responsible for binding to PD-1, and this interaction has been demonstrated through various biochemical experiments, including structural studies[32,33], binding assays[34], and the use of inhibitors or antibodies targeting the IgV-like domain[35–37]. We also used AlphaFold 3 to predict that the deletion of the IgV-like domain would lead to a significant decrease in the interacting protein docking (Fig. 5D). This suggests that *P. gingivalis* can utilize gingipain to influence the AS of PD-L1 in macrophages. By increasing the expression of the IgV-like domain, it enhances the interaction between PD-L1 and PD-1, leading to T cell suppression. This mechanism allows gingipain to promote immune evasion, supporting its survival (Fig. 6).

◀**Fig. 3**. Infection of macrophages by gingipain-expressing *P. gingivalis* upregulated PD-L1 containing the IgV-like domain. (**A**) Western blot analysis showing the expression levels of PD-L1 and *β*-actin in macrophages infected with *P. gingivalis* or its gingipain-deficient mutant (*ΔKDP*). Proteins were extracted from macrophages and resolved on 10% SDS-PAGE gels (4 µg of protein per lane). The proteins were transferred to PVDF membranes and probed with specific antibodies against PD-L1 and *β*-actin. The same set of samples was analyzed in two separate experiments to ensure consistency. (**B**) Densitometric analysis of PD-L1 expression normalized to *β*-actin. The graph represents the mean ± *SD* of three independent biological replicates. Statistical analysis was performed using one-way ANOVA with Tukey's test. (**C**) RT-PCR products showing the exon structures of PD-L1 isoforms. Lane 1: 100 bp DNA ladder. Lane 2: RT-PCR product from total RNA of No-inf macrophages. To the right, exon structures of PD-L1^{IgV-} isoform (805 bp), non-coding isoform (632 bp), and PD-L1^{IgV+} isoform (483 bp) are shown. The forward and reverse primers used for amplification are indicated. (**D**–**E**) RT-qPCR analysis of PD-L1 RNA expression levels (normalized to *β*-actin) in No-inf, *Pg*-inf, and *ΔKDP*-inf macrophages. (**F**) Percent spliced in (PSI) analysis of PD-L1 isoforms in No-inf, *Pg*-inf, and *ΔKDP*-inf macrophages based on the result in Fig. S1B. Statistical analysis was performed using one-way ANOVA for (**B**, **D**–**E**) and two-way ANOVA for (**F**). Data in (**B**) are presented as mean ± *SD* from three independent biological replicates. Data in (**D**–**F**) are presented as mean ± *SD* from five independent biological replicates. Significant differences are indicated as follows: $^{*}p < 0.05$, $^{**}p < 0.01$, $^{***}p < 0.005$, $^{****}p < 0.001$. The *p*-values for non-significant differences are displayed separately.

Macrophages undergo numerous AS changes during their differentiation and activation in vitro, influencing their roles in detection, phagocytosis, and cytokine secretion[38]. The occurrence of these AS events is mainly attributed to two factors. First, host cells produce splice variants to inhibit the invasion and replication of microbes[39,40]. Second, microbial infections result in the production of aberrant isoforms of antiviral genes to facilitate the invasion and replication of pathogens[41]. Through comparative analysis from sequence results of No-inf, *Pg*-inf, and *ΔKDP*-inf, we had observed a lot of Sig. AS events in macrophages that following infection (Fig. 1B). These AS events were categorized into 18 patterns based on the different kinds of isoform switches (Fig. 1C), which can be further classified into four major categories: (1) Isoform switching events that remain unchanged during infection, including "IDR with binding region loss or gain"; (2) Isoform switching events that change during infection but are unrelated to gingipain, including "3'UTR is shorter or longer", "Complete ORF loss or gain", "IDR loss or gain", "Length loss or gain", and "Signal peptide loss or gain"; (3) Isoform switching events that change during infection and are directly influenced by gingipain, including "Domain loss or gain", "Exon loss or gain", "IDR length loss or gain", "Transcript is noncoding or coding", and "TSS more upstream or downstream"; (4) Isoform switching events that occur only in the absence of gingipain during infection, or in other words, gingipain can inhibit the occurrence of these isoform switching events, including "5'UTR is shorter or longer", "Domain length loss or gain", "Intron retention (IR) loss or gain", "Last exon more upstream or downstream", "NMD sensitive or insensitive", and "TTS more upstream or downstream".

Hereafter, we focused on the latter two categories of AS changes related to gingipain. In the category of AS regulated by gingipain, we found that gingipain influences AS in macrophages by affecting exon inclusion or exclusion in transcripts and even causing the gain or loss of entire protein domains. These changes may directly impact immune cell function. For example, the integrity of the IFNα/β receptor protein structure is closely related to many human immune-related diseases[42]; the loss of certain N-terminal domains of short FOXP1 ($FOXP1_S$) affects its interaction with downstream proteins or molecules, thereby influencing B cell maturation and function[43]; the generation of NIRP3 isoforms lacking exon 5 leads to a loss of interaction with NIMA related Kinase 7 (NEK7) and its activity, which in turn affects the innate immune response in vertebrates[44]. Similarly, in our study, we found that the loss of the IgV-like domain of PD-L1 due to *P. gingivalis* infection, which affects its efficiency in binding to PD-1, also falls into this category (Fig. 1C).

Additionally, we found gingipain also regulated AS in macrophages by increasing or decreasing the number of translatable transcripts, which also impacts the function of immune cells. For example, after *Mycobacterium tuberculosis* (*Mtb*) infection in macrophages, the number of non-translatable isoforms increases, which correlates with the reduction in many cellular protein levels and affects macrophage maturation[45]. Meanwhile, we found that gingipain can inhibit certain AS events in macrophages, which are closely related to immune cell functions during inflammation. For instance, under stimulation by the inflammatory cytokine LPS, human Interferon regulatory factor-5 (IRF-5) transcribes five types of longer 5'UTR, which are involved in subsequent normal inflammation[46]; the Nonsense-mediated mRNA decay (NMD) mechanism plays a crucial role in degrading abnormal immunoglobulin and T Cell Receptor (TCR) transcripts in lymphocytes[47]; the dynamic balance of splicing factors and the level of IR are closely related to B cell differentiation[48]. However, these AS changes, which are essential during inflammation, may potentially be inhibited by gingipain.

The elevation of surface PD-L1 protein expression by *P. gingivalis* via gingipain has previously been confirmed in dendritic cells[31]. Both macrophages and dendritic cells are capable of presenting antigens to T cells, though macrophages possess stronger phagocytic abilities. Typically, monocytes, which differentiate into macrophages at infection sites, use macropinocytosis to ingest nutrients, pathogens, soluble antigens, and large extracellular molecules[49]. However, *P. gingivalis* can survive for extended periods after being phagocytosed by macrophages[50]. Our previous work demonstrated the presence of live *P. gingivalis* within macrophages 24 to 48 h post-infection[8], suggesting that phagocytosed *P. gingivalis* can persist and influence intracellular biochemical processes, such as DNA replication, RNA transcription, and protein translation or modification.

P. gingivalis is a major pathogen of periodontitis[51], which has been linked to various systemic conditions such as diabetes mellitus[52,53], rheumatoid arthritis[54], and Alzheimer's disease[55]. The dissemination of *P. gingivalis*

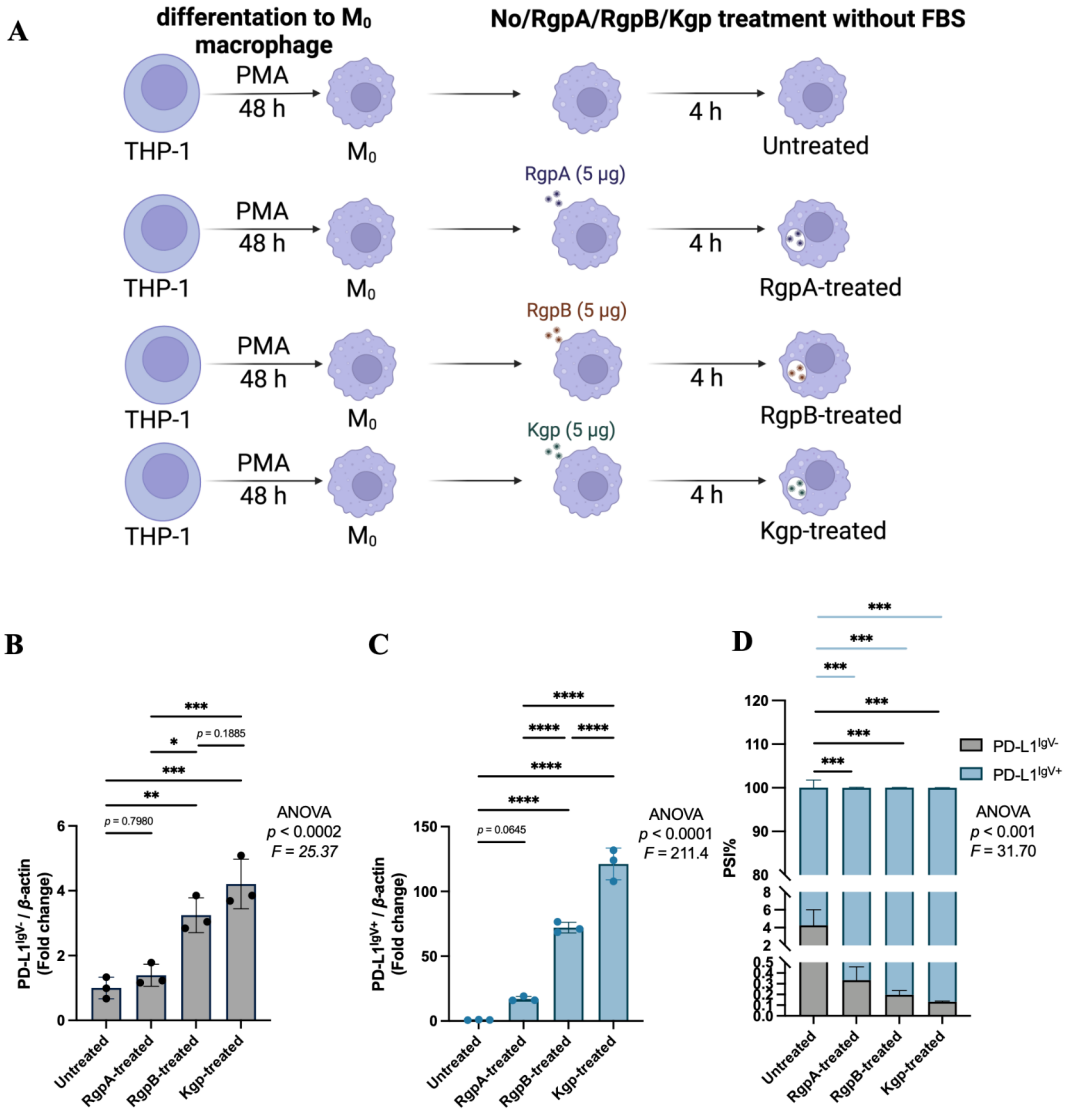

Fig. 4. Recombinant gingipain upregulated PD-L1 isoform containing the IgV-like domain in macrophages. (**A**) Workflow for establishing of Untreated, RgpA-treated, RgpB-treated and Kgp-treated macrophages. (**B**–**C**) RT-qPCR analysis of PD-L1 RNA expression levels (normalized to *β*-actin) in Untreated, RgpA-treated, RgpB-treated and Kgp-treated macrophages with 5 μg/mL in PBS for 4 h. (**D**) Percent spliced in (PSI) analysis of PD-L1 isoforms in Untreated, RgpA-treated, RgpB-treated and Kgp-treated macrophages 5 μg/mL in PBS for 4 h based on the result in Fig. S1B. Statistical analysis was performed using one-way ANOVA for (**B**–**C**) and two-way ANOVA for (**D**). Data in (**B**-**D**) are presented as mean ± *SD* from three independent biological replicates. Significant differences are indicated as follows: $^{*}p < 0.05$, $^{**}p < 0.01$, $^{***}p < 0.005$, $^{****}p < 0.001$. The *p*-values for non-significant differences are displayed separately.

to various systemic organs is facilitated by its secretion of outer membrane vesicles (OMVs)[56,57], which carry various virulent factors throughout the body *via* blood circulation[58,59]. Gingipains help *Pg* evade the immune system by degrading junctional adhesion molecule (JAM1) on gingival epithelial cells, disrupting the epithelial barrier[5], and degrading key innate immune components such as defensins and complement proteins[59–61]. In this study, by analyzing changes in AS of certain genes in macrophages after *P. gingivalis* infection, we identified a subset of genes associated with gingipains. Among these genes, we found a significant increase in the functional isoform of PD-L1, which is closely related to the inhibition of T cell function. This provides a theoretical basis for gingipains affecting the host's adaptive immunity by inhibiting T cell activation helping *P. gingivalis* achieve immune evasion.

The mechanism by which gingipain, a unique toxic protease from *P. gingivalis*, participates in the nucleic acid-driven process remains unclear. AS, a process transitioning pre-mRNA to mature mRNA, requires the participation of multiple proteins, either directly or indirectly. Central to this process are small nuclear ribonucleoproteins (snRNPs), which form essential components of the spliceosome[62]. Additionally, RNA-binding proteins (RBPs) indirectly regulate AS[63]. Although our sequencing data did not show significant changes

in snRNP expression in macrophages following *P. gingivalis* infection, we observed a marked reduction in the expression of RNA Binding Protein with Multiple Splicing (RBPMS), as shown in our sequencing results (https://d3dcaz4rv8jgb4.cloudfront.net/). In *Pg*-inf macrophages, RBPMS expression dropped to 11.2% of that in No-inf macrophages and 17.6% of that in *ΔKDP*-infected macrophages. This suggests that *P. gingivalis* infection may lead to a decrease in RBPMS in macrophages, and this phenomenon may be related to gingipain. Previous studies have demonstrated that RBPMS is closely linked to exon skipping during AS[64–66]. This aligns with our observation that *P. gingivalis* infection leads to a decrease in the exon 3 (IgV-like domain) skipping during the AS of PD-L1. However, the relationship between gingipain and RBPMS still requires further validation. Additionally, whether the decrease in RBPMS is related to the increase in the IgV-like domain of PD-L1 also needs to be further investigated.

Overall, this study demonstrated that gingipains selectively increase the expression of PD-L1^{IgV+} in macrophages by regulating the AS during *P. gingivalis* infection, providing a potential mechanism for immune evasion by *P. gingivalis* in the host. These findings could be important for understanding the mechanisms of *P. gingivalis* immune evasion and may be beneficial for establishing pharmacological therapies for the infection of *P. gingivalis*.

Methods

Bacterial culture

Normal (strain ATCC33277) and *P. gingivalis* with all three gingipains (RgpA, RgpB, and Kgp) knocked out (strain *ΔKDP*) (Nagasaki University, Japan)[67] were cultured anaerobically at 37 °C in Brain Heart Infusion medium (237500, Becton Dickinson, USA) supplemented with 1 mg/mL L-Cysteine (033-20655, Wako, Japan), 10 μg/mL hemin (5180-1G, Sigma-Aldrich, Japan), 1 μg/mL 2-methyl-1,4-naphthoquinone (vitamin K3) (M9A1503, Nacalai Tesque, Japan).

Cell culture

The THP-1 human monocytic cell line purchased from RIKEN Cell Bank RCB 1189 Tsukuba TOHOKU was seeded at a concentration of 30,000 cells/mL and cultured in RPMI 1640 supplemented with 10% FBS at 37 °C in 5% CO_2.

Bacterial infection

At 24 h post-seeding, THP-1 cells were differentiated into macrophages by treatment with 100 nM phorbol myristate acetate for 48 h. The differentiated THP-1 cells were then exposed to *P. gingivalis* (MOI = 100) or *ΔKDP* (MOI = 100) for 4 h in RPMI 1640 supplemented with 10% FBS. After incubation, unbound *P. gingivalis* and *ΔKDP* were removed by washing with PBS. The *Pg*-infected and *ΔKDP*-infected macrophages were then incubated for 48 h in RPMI 1640 containing 10% FBS and 1% penicillin/streptomycin. The harvested macrophages were subsequently used for RNA and protein extraction.

Gingipain treatment

At 24 h post-seeding, THP-1 cells were differentiated into macrophages by treatment with 100 nM phorbol myristate acetate for 48 h. The differentiated THP-1 cells were then treated separately with recombinant gingipains from *P. gingivalis* (RgpA, #CSB-EP338957PQP, CUSABIO TECHNOLOGY, Wuhan, China; RgpB, #CSB-EP310587EYA(A4), CUSABIO TECHNOLOGY, Wuhan, China; Kgp, #CSB-EP464342EXZ, CUSABIO TECHNOLOGY, Wuhan, China) at a concentration of 5 μg/mL, diluted in PBS, and incubated for 4 h in RPMI 1640 medium. Following treatment, macrophages were washed with PBS and harvested for RNA extraction.

Libraries preparation and sequencing

RNA extraction from each sample was performed using the RNeasy Mini Kit (QIAGEN). The concentration of the obtained total RNA was measured using NanoDrop ONE, resulting in total yields of 11.3 μg for No-inf, 4.4 μg for *Pg*-inf, and 4.5 μg for *ΔKDP*-inf. Total RNA (50 ng) was subjected to poly(A) RNA extraction and fragmentation using the NEBNext Poly(A) mRNA Magnetic Isolation Module (NEB) and the NEBNext Ultra II RNA Library Prep Kit for Illumina (NEB), following the protocol outlined in the NEBNext Ultra II RNA Library Prep Kit for Illumina Instruction Manual. Fragmentation was achieved by adding NEBNext First Strand Synthesis Reaction Buffer and NEBNext Random Primers to the NEBNext Ultra II RNA Library Prep Kit for Illumina (NEB), followed by incubation at 94 °C for 15 min. The fragmented poly(A) RNA was subjected to reverse transcription using the NEBNext First Strand Synthesis Enzyme Mix from the NEBNext Ultra II RNA Library Prep Kit for Illumina (NEB), followed by the addition of NEBNext Adaptor (NEB) to generate cDNA. The prepared cDNA was amplified by PCR to generate libraries. To identify the samples, barcode sequences No-inf (10 μg/uL), *Pg*-inf (15.2 μg/uL) and *ΔKDP*-inf (10.3 μg/uL) were added using NEBNext Multiplex Oligos for Illumina. Furthermore, analysis was conducted using the Bioanalyzer to confirm the distribution of library lengths. The analysis results indicated that libraries of the desired lengths were prepared, and sufficient concentration and purity were observed, thus proceeding with next-generation sequencing analysis.

Bioinformatic analysis of bulk RNA-seq data

After quality trimming with Trim Galore v0.6.10, the reads were aligned to the GRCm38.108 reference genome (Ensembl Release 108) using the STAR aligner v2.7.10b. De novo transcript assembly and annotation were performed using StringTie v2.2.1 and SQANTI3 v5.0. Transcript-level quantification was performed for all samples using Salmon v1.9.0, followed by further quality filtering with isoformSwitchAnalyzeR v1.17.05, based on Salmon's mapping results.

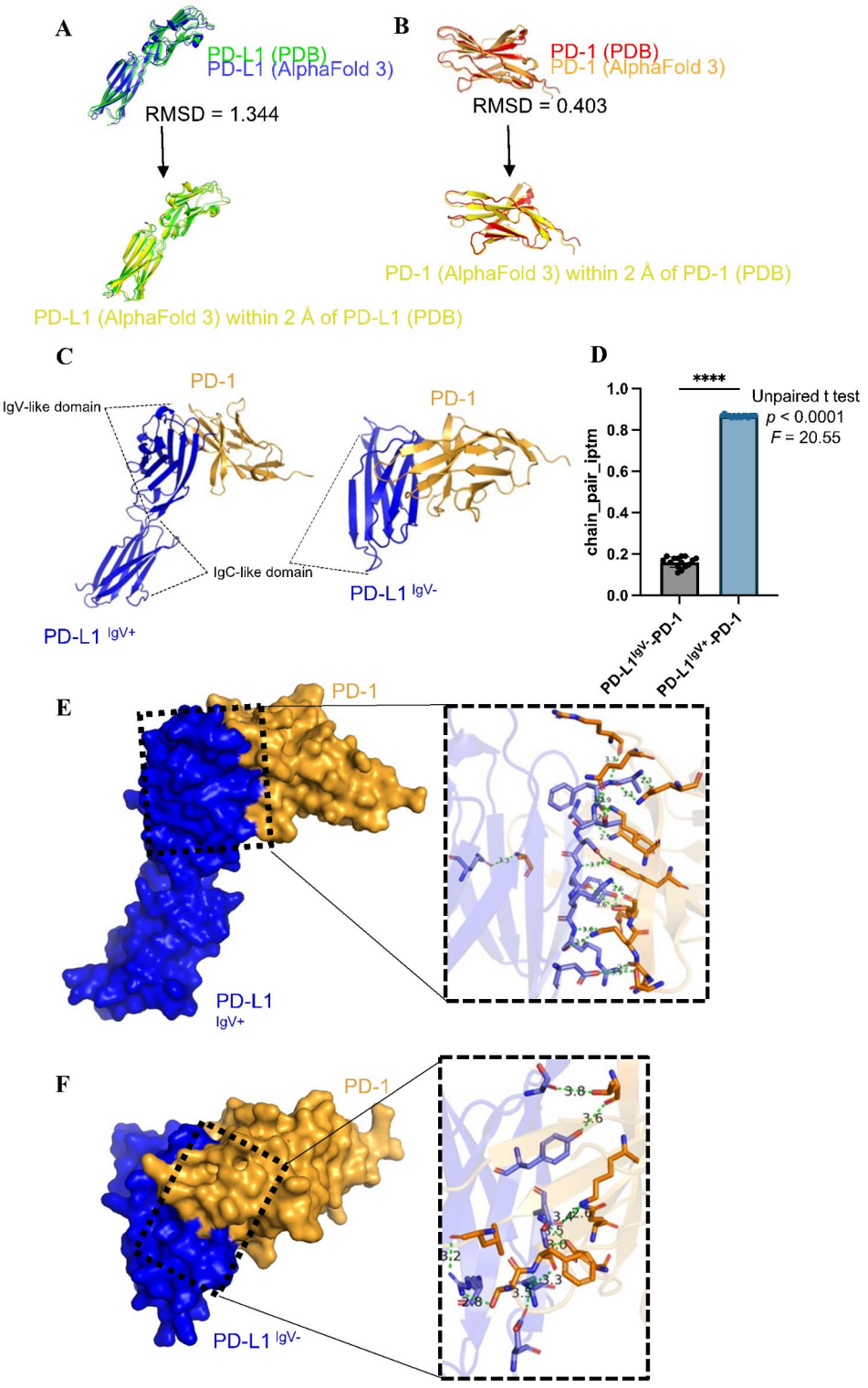

Differentially expressed genes were identified using DESeq2 v1.31.16, with DEGs defined by a False Discovery Rate < 0.05 and |log2Fold Change| > 1. The core default statistical method was the Wald test. The *p*-values obtained are corrected using the Benjamini-Hochberg method to control the FDR in the context of multiple testing.

Significant differential exon usage was detected by DEXSeq v1.44.0 within the IsoformSwitchAnalyzeR v1.17.05. In the analysis of RNA-seq data, DEU was determined by DEXSeq through the comparison of full and reduced models via the Likelihood Ratio Test. The *p*-values obtained are corrected using the Benjamini-Hochberg method to control the FDR in the context of multiple testing.

Additionally, Gene Ontology (GO) enrichment analysis was performed using clusterProfiler v4.6.0.ss.

◀**Fig. 5**. Comparison of PD-L1^{IgV+} and PD-L1^{IgV-} binding to PD-1 based on Alphafold 3 prediction, showing enhanced binding of PD-L1^{IgV+}. (**A**) The aligned model of PD-L1 protein structure RCSB PDB database (green) and corresponding AlphaFold predicted protein structure (blue) is shown. RMSD = 1.34. The yellow-highlighted regions within PD-L1 protein structure predicted by AlphaFold 3 indicate parts with less than a 2 Å deviation compared to the PD-L1 protein structure from the RCSB PDB database. (**B**) The align model of PD-1 protein structure from PDB database (red) and corresponding AlphaFold predicting protein structure (orange) is shown. RMSD = 0.403. The yellow-highlighted regions within PD-1 protein structure predicted by AlphaFold 3 indicate the parts with less than 2 Å deviation compared to the PD-1 protein structure from the PDB database. (**C**) AlphaFold 3 predicted model of PD-L1^{IgV+}-PD-1 (Left) and PD-L1^{IgV-}-PD-1. (**D**) The chain_pair_iptm of AlphaFold 3 predicted models of PD-L1^{IgV+}-PD-1 ($n = 15$) and PD-L1^{IgV-}-PD-1 ($n = 15$). (**E**) Zoomed-in cartoon view of the PD-L1^{IgV+}- PD-1 interface with Hydrogen bonds (green). (**F**) Zoomed-in cartoon view of the PD-L1^{IgV-}- PD-1 interface with Hydrogen bonds (green). $^{****}p < 0.001$.

SDS-PAGE and Western blot analysis

The No-inf, *Pg*-inf, and *ΔKDP*-inf macrophage cells were harvested into lysis buffer, subjected to SDS-PAGE, and then transferred onto PVDF membranes (Merck, Darmstadt, Germany). Primary antibodies included a PD-L1 mouse monoclonal antibody (1:500, 405.9A11, Cell Signaling Technology, USA) and *β*-actin (1:1000, 3700 S, Cell Signaling Technology, USA). Following incubation with primary antibodies overnight, membranes were washed with TBST for 30 min at room temperature and subsequently incubated with an anti-mouse IgG HRP-linked secondary antibody (1:10000, #7076, Cell Signaling Technology) for 45 min at room temperature. Finally, signals were detected using Western Blot Chemiluminescence HRP Substrate (WBLUF0100; Millipore, Burlington, MA, USA). Densitometric analysis of the bands was performed using ImageJ (National Institutes of Health, Bethesda, MD, USA).

Reverse transcription polymerase chain reaction (RT-PCR)

RNA was extracted using Trizol reagent (Invitrogen). The PrimeScript Reverse Transcription kit (Takara) was used for reverse transcription of the total RNA. In the 10 µL reverse transcription system, 2 µL of RNA at a concentration of 500 ng/µL was used (total 1 µg), resulting in a final cDNA concentration of 100 ng/µL. The cDNA served as a template for RT-PCR using GoTaq® Green Master Mix (LOT 0000471784, Promega, USA). For amplification of PD-L1, RT-PCR was performed using 200 ng template cDNA with an initial denaturation for 2 min at 95 °C, followed by 40 cycles of 95 °C for 30 s, 60 °C for 30 s, 72 °C for 1 min, and a final extension for 10 min at 72 °C. The primers for different lengths of PD-L1 isoforms are as follows: PD-L1-forward, 5'- CCT ACT GGC ATT TGC TGA ACG – 3'; PD-L1-reverse, 5'- GAG TTT GTA TCT TGG ATG CCA CAT T-3'. All primers were designed by NIH Primer-BLAST (https://www.ncbi.nlm.nih.gov/tools/primer-blast/).

Reverse transcription-quantitative polymerase chain reaction (RT-qPCR)

cDNA products were the same with previous RT-PCR method. The resulting cDNA products were diluted two-fold with pure water, and 2 µL of the diluted cDNA (total 100 ng) was used as a template for quantifying the relative RNA content via RT-qPCR using Luna Universal qPCR Master Mix (#M3003E, New England Biolabs Inc., MA). Relative levels of PCR products were determined using a LightCycler System (Roche Diagnostics, Mannheim, Germany), with the threshold cycle (Ct) automatically determined using default settings on the LightCycler 96 software (version 1.1; Roche Diagnostics, Mannheim, Germany). The primers for each target isoform were as follows: *β*-actin-forward, 5'-TGG CAC CCA GCA CAA TGA A-3'; *β*-actin-reverse, 5'-CTA AGT CAT AGT CCG CCT AGA AG C-3'; PD-L1^{IgV-}-forward, 5'-TTT GCT GAA CGC CCC ATA CA-3' or 5'-TTG CTG AAC GCC CCA TAC AA-3'; PD-L1^{IgV-}-reverse, 5'-TGC TTG TCC AGA TGA CTT CGG-3'; PD-L1^{IgV+}-forward, 5'-TAC TGT CAC GGT TCC CAA GGA-3'; PD-L1^{IgV+}-reverse, 5'-TGA TTC TCA GTG TGC TGG TCA-3'. All primers were designed as before in RT-PCR methods section. Differences in gene expression levels were calculated using the $2^{-\Delta Ct}$ and $2^{-\Delta\Delta Ct}$ methods after normalization of target gene expression levels within each sample against the expression levels of the reference gene (*β*-actin).

AlphaFold 3 prediction

We used the protein prediction software AlphaFold 3 to predict the protein complexes formed by PD-L1^{IgV-} and PD-L1^{IgV+} with PD-1, respectively. Specifically, we used the AlphaFold 3 server (https://alphafoldserver.com/)[68] and input the sequences for human PD-L1$^{IgV-/IgV+}$ and PD-1 from the RCSB PDB database (https://www.rcsb.org) as follows: IgV-like domain is from 4ZQK (AA18-132); PD-L1^{IgV-} is from 3BIK (AA133-229); PD-L1^{IgV+} is from 3BIK (AA18-229); and PD-1 is from 3RRQ (AA31-149). The accuracy of the AlphaFold 3 model was evaluated by Root Mean Square Deviation (RMSD) values between the protein structures predicted by AlphaFold 3 and the structures downloaded from the RCSB PDB database[69]. By analyzing the chain_pair_iptm scores of the 15 PD-L1 and PD-1 complexes generated from three independent AlphaFold 3 predictions (5 models per prediction), we evaluated the confidence of the predicted protein-protein interfaces. All modifications and comparisons of the protein structures in this study were performed using PyMOL (3.0.3). Hydrogen bonds formed in protein docking were predicted using the PDBePISA tool from EMBL-EBI (https://www.ebi.ac.uk/pdbe/pisa/).

Statistical analysis

Western blot density analysis in Fig. 3B and RT-qPCR $2^{-\Delta\Delta Ct}$ values in Fig. 4B–C were analyzed by ordinary one-way analysis of variance with Tukey's multiple comparisons test. RT-qPCR $2^{-\Delta Ct}$ values in Fig. S3 were analyzed

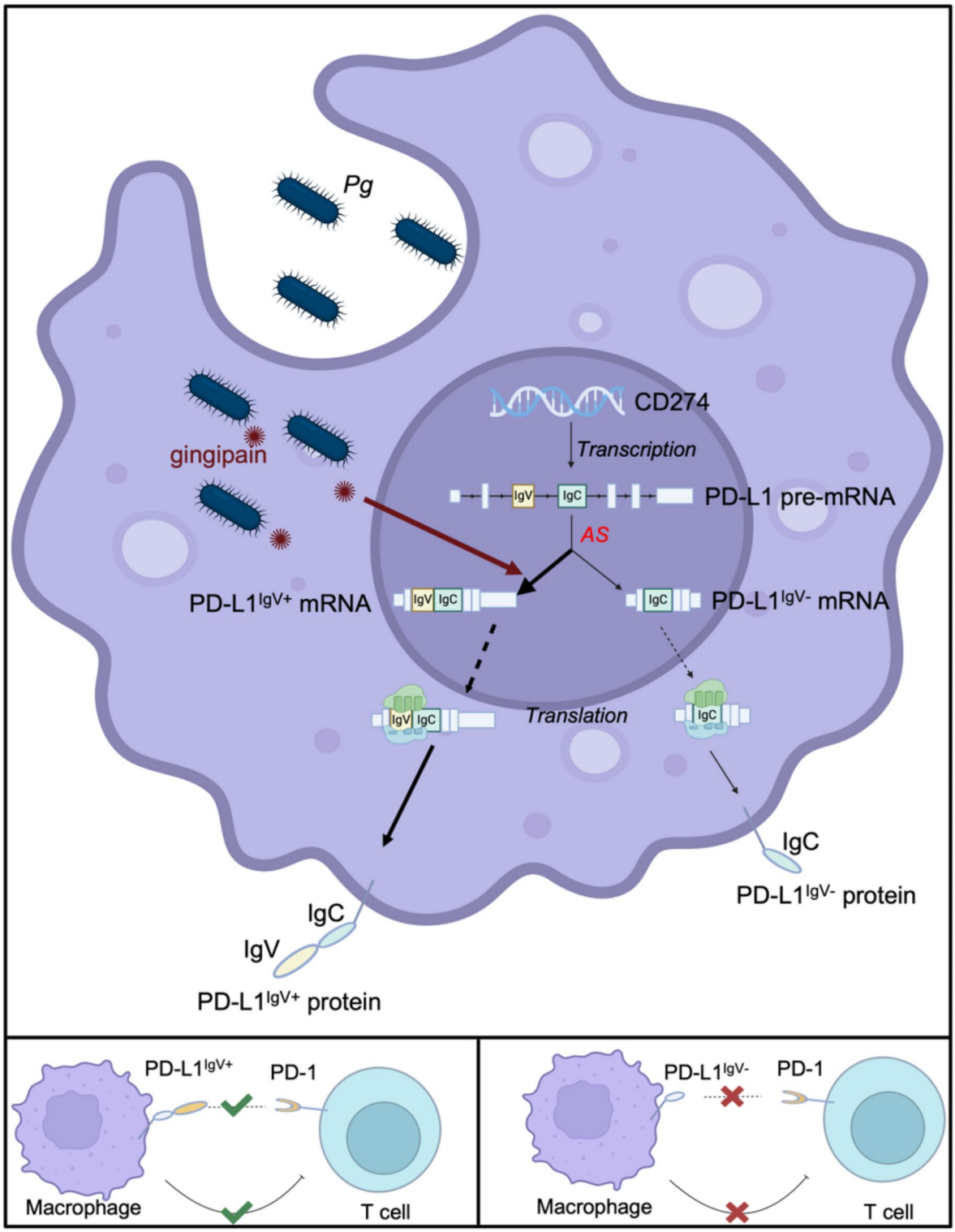

Fig. 6. Mechanism of PD-L1 AS in macrophages modulated by gingipains derived from *P. gingivalis*. *P. gingivalis* infection and gingipain release influence PD-L1 AS in macrophages. The PD-L1^{IgV+} isoform, primarily upregulated by *P. gingivalis*, retains both IgV and IgC-like domains, which allowing it to bind to PD-1 on T cells and suppressing immune responses.

by two-way ANOVA with Tukey's multiple comparisons test. Percent spliced in (PSI) in Fig. 4D was analyzed by two-way ANOVA with Šídák's multiple comparisons test. Chain_pair_iptm values in Fig. 5D were analyzed by unpaired t test. In all the above statistical analyses, comparisons were performed using GraphPad Prism 9 for Mac. Significance was considered as follows: $^{*}p < 0.05$; $^{**}p < 0.01$; $^{***}p < 0.005$; $^{***}p < 0.001$.

Data availability

The sequencing data generated during this study are available in the NCBI BioProject repository under the accession number PRJNA1163056. The associated metadata can be accessed via the following link: https://dataview.ncbi.nlm.nih.gov/object/PRJNA1163056?reviewer=clcri79f3dn6h4oicc0g5lhlsi . The data analysis results for this study are presented at the following link: https://d3dcaz4rv8jgb4.cloudfront.net/.

Received: 7 November 2024; Accepted: 18 March 2025
Published online: 26 March 2025

References

1. Socransky, S. S., Haffajee, A. D., Cugini, M. A., Smith, C. & Kent, R. L. Jr. Microbial complexes in subgingival plaque. *J. Clin. Periodontol.* **25**, 134–144. https://doi.org/10.1111/j.1600-051x.1998.tb02419.x (1998).
2. Lamont, R. J. & Jenkinson, H. F. Life below the gum line: pathogenic mechanisms of *Porphyromonas gingivalis*. *Microbiol. Mol. Biol. Rev.* **62**, 1244–1263. https://doi.org/10.1128/mmbr.62.4.1244-1263.1998 (1998).
3. Potempa, J., Pike, R. & Travis, J. Titration and mapping of the active site of cysteine proteinases from *Porphyromonas gingivalis* (gingipains) using peptidyl chloromethanes. *Biol. Chem.* **378**, 223–230. https://doi.org/10.1515/bchm.1997.378.3-4.223 (1997).
4. Uitto, V. J., Larjava, H., Heino, J. & Sorsa, T. A protease of bacteroides gingivalis degrades cell surface and matrix glycoproteins of cultured gingival fibroblasts and induces secretion of collagenase and plasminogen activator. *Infect. Immun.* **57**, 213–218. https://doi.org/10.1128/iai.57.1.213-218.1989 (1989).
5. Takeuchi, H. et al. Porphyromonas gingivalis induces penetration of lipopolysaccharide and peptidoglycan through the gingival epithelium via degradation of junctional adhesion molecule 1. *PLoS Pathog.* **15**, e1008124. https://doi.org/10.1371/journal.ppat.1008124 (2019).
6. Kitamura, Y., Matono, S., Aida, Y., Hirofuji, T. & Maeda, K. Gingipains in the culture supernatant of *Porphyromonas gingivalis* cleave CD4 and CD8 on human T cells. *J. Periodontal Res.* **37**, 464–468. https://doi.org/10.1034/j.1600-0765.2002.01364.x (2002).
7. Glowczyk, I. et al. Inactive gingipains from *P. gingivalis* selectively skews T cells toward a Th17 phenotype in an IL-6 dependent manner. *Front. Cell. Infect. Microbiol.* **7**, 140. https://doi.org/10.3389/fcimb.2017.00140 (2017).
8. Yoshida, K. et al. Extracellular vesicles of *P. gingivalis*-infected macrophages induce lung injury. *Biochim. Biophys. Acta Mol. Basis Dis.* **1867**, 166236. https://doi.org/10.1016/j.bbadis.2021.166236 (2021).
9. Zhou, H. L., Luo, G., Wise, J. A. & Lou, H. Regulation of alternative splicing by local histone modifications: potential roles for RNA-guided mechanisms. *Nucleic Acids Res.* **42**, 701–713. https://doi.org/10.1093/nar/gkt875 (2014).
10. Luco, R. F. et al. Regulation of alternative splicing by histone modifications. *Science* **327**, 996–1000. https://doi.org/10.1126/science.1184208 (2010).
11. Pan, Q., Shai, O., Lee, L. J., Frey, B. J. & Blencowe, B. J. Deep surveying of alternative splicing complexity in the human transcriptome by high-throughput sequencing. *Nat. Genet.* **40**, 1413–1415. https://doi.org/10.1038/ng.259 (2008).
12. Hong, W. et al. The role of mRNA alternative splicing in macrophages infected with Mycobacterium tuberculosis: A field needing to be discovered. *Molecules* **29**(8), 1798. https://doi.org/10.3390/molecules29081798 (2024).
13. Huang, P., Wen, F., Tuerhong, N., Yang, Y. & Li, Q. Neoantigens in cancer immunotherapy: Focusing on alternative splicing. *Front. Immunol.* **15**, 1437774. https://doi.org/10.3389/fimmu.2024.1437774 (2024).
14. Bashraheel, S. S., Al-Sulaiti, H. & Goda, S. K. Generation of novel Tumour-Selective SEA Superantigen-Based peptides with improved safety and efficacy for precision cancer immunotherapy. *Int. J. Mol. Sci.* **25**(17), 9423. https://doi.org/10.3390/ijms25179423 (2024).
15. Zak, K. M. et al. Structural biology of the immune checkpoint receptor PD-1 and its ligands PD-L1/PD-L2. *Structure* **25**, 1163–1174. https://doi.org/10.1016/j.str.2017.06.011 (2017).
16. Yi, M. et al. Combination strategies with PD-1/PD-L1 Blockade: Current advances and future directions. *Mol. Cancer*. **21**, 28. https://doi.org/10.1186/s12943-021-01489-2 (2022).
17. Seliger, B. Basis of PD1/PD-L1 therapies. *J. Clin. Med.* **8**(12), 2168. https://doi.org/10.3390/jcm8122168 (2019).
18. He, X. H., Xu, L. H. & Liu, Y. Identification of a novel splice variant of human PD-L1 mRNA encoding an isoform-lacking Igv-like domain. *Acta Pharmacol. Sin*. **26**, 462–468. https://doi.org/10.1111/j.1745-7254.2005.00086.x (2005).
19. Lee, H. T. et al. Molecular mechanism of PD-1/PD-L1 blockade via anti-PD-L1 antibodies Atezolizumab and durvalumab. *Sci. Rep.* **7**, 5532. https://doi.org/10.1038/s41598-017-06002-8 (2017).
20. Kundapura, S. V. & Ramagopal, U. A. The CC' loop of IgV domains of the immune checkpoint receptors, plays a key role in receptor: Ligand affinity modulation. *Sci. Rep.* **9**, 19191. https://doi.org/10.1038/s41598-019-54623-y (2019).
21. Zhou, J., Ma, S., Wang, D., Zeng, J. & Jiang, T. FreePSI: an alignment-free approach to estimating exon-inclusion ratios without a reference transcriptome. *Nucleic Acids Res.* **46**, e11. https://doi.org/10.1093/nar/gkx1059 (2018).
22. Nagano, K. et al. Characterization of raga and RagB in *Porphyromonas gingivalis*: Study using gene-deletion mutants. *J. Med. Microbiol.* **56**, 1536–1548. https://doi.org/10.1099/jmm.0.47289-0 (2007).
23. Betancourt, M. R. & Skolnick, J. Universal similarity measure for comparing protein structures. *Biopolymers* **59**, 305–309. (2001).
24. Maiorov, V. N. & Crippen, G. M. Size-independent comparison of protein three-dimensional structures. *Proteins* **22**, 273–283. https://doi.org/10.1002/prot.340220308 (1995).
25. Launay, R. et al. Structural reconstruction of *E. coli* Ubi metabolon using an AlphaFold2-Based computational framework. *J. Chem. Inf. Model.* **64**, 5175–5193. https://doi.org/10.1021/acs.jcim.4c00304 (2024).
26. Hoos, A. Development of immuno-oncology drugs: From CTLA4 to PD1 to the next generations. *Nat. Rev. Drug Discov*. **15**, 235–247. https://doi.org/10.1038/nrd.2015.35 (2016).
27. Shin, D. S. & Ribas, A. The evolution of checkpoint Blockade as a cancer therapy: what's here, what's next? *Curr. Opin. Immunol.* **33**, 23–35. https://doi.org/10.1016/j.coi.2015.01.006 (2015).
28. Sharma, P. & Allison, J. P. The future of immune checkpoint therapy. *Science* **348**, 56–61. https://doi.org/10.1126/science.aaa8172 (2015).
29. Adel-Khattab, D. et al. Porphyromonas gingivalis induced up-regulation of PD-L1 in colon carcinoma cells. *Mol. Oral Microbiol.* **36**, 172–181. https://doi.org/10.1111/omi.12332 (2021).
30. Groeger, S. et al. PD-L1 Up-Regulation in prostate cancer cells by *Porphyromonas gingivalis*. *Front. Cell. Infect. Microbiol.* **12**, 935806. https://doi.org/10.3389/fcimb.2022.935806 (2022).
31. Ren, J. et al. Gingivalis infection upregulates PD-L1 expression on dendritic cells, suppresses CD8 + T-cell responses, and aggravates oral cancer. *Cancer Immunol. Res.* **11**, 290–305. https://doi.org/10.1158/2326-6066.Cir-22-0541 (2023).
32. Slater, B. T., Han, X., Chen, L. & Xiong, Y. Structural insight into T cell coinhibition by PD-1H (VISTA). *Proc. Natl. Acad. Sci. U S A* **117**, 1648–1657. https://doi.org/10.1073/pnas.1908711117 (2020).
33. Walker, K., Waters, L. C., Kelly, G., Muskett, F. W. & Carr, M. D. Sequence-specific (1)H, (13)C and (15)N backbone NMR assignments for the N-terminal IgV-like domain (D1) and full extracellular region (D1D2) of PD-L1. *Biomol. NMR Assign.* **16**, 281–288. https://doi.org/10.1007/s12104-022-10092-5 (2022).

34. Chaudhri, A. et al. PD-L1 binds to B7-1 only in Cis on the same cell surface. *Cancer Immunol. Res.* **6**, 921–929. https://doi.org/10.1158/2326-6066.Cir-17-0316 (2018).
35. Martínez-Vicente, P. et al. Discovery of the first PD-1 ligand encoded by a pathogen. *Front. Immunol.* **13**, 1007334. https://doi.org/10.3389/fimmu.2022.1007334 (2022).
36. Kitel, R. et al. Exploring the surface of the ectodomain of the PD-L1 immune checkpoint with small-molecule fragments. *ACS Chem. Biol.* **17**, 2655–2663. https://doi.org/10.1021/acschembio.2c00583 (2022).
37. Kang-Pettinger, T. et al. Identification, binding, and structural characterization of single domain anti-PD-L1 antibodies inhibitory of immune regulatory proteins PD-1 and CD80. *J. Biol. Chem.* **299**, 102769. https://doi.org/10.1016/j.jbc.2022.102769 (2023).
38. Liu, H. et al. Alternative splicing analysis in human monocytes and macrophages reveals MBNL1 as major regulator. *Nucleic Acids Res.* **46**, 6069–6086. https://doi.org/10.1093/nar/gky401 (2018).
39. Savan, R. Alternative splicing in innate antiviral immunity. *J. Interferon Cytokine Res.* **38**, 317–318. https://doi.org/10.1089/jir.2018.29010.rsa (2018).
40. Haque, N., Ouda, R., Chen, C., Ozato, K. & Hogg, J. R. ZFR coordinates crosstalk between RNA decay and transcription in innate immunity. *Nat. Commun.* **9**, 1145. https://doi.org/10.1038/s41467-018-03326-5 (2018).
41. Pozzi, B. et al. Dengue virus targets RBM10 deregulating host cell splicing and innate immune response. *Nucleic Acids Res.* **48**, 6824–6838. https://doi.org/10.1093/nar/gkaa340 (2020).
42. de Weerd, N. A., Vivian, J. P., Lim, S. S., Huang, S. U. & Hertzog, P. J. Structural integrity with functional plasticity: What type I IFN receptor polymorphisms reveal. *J. Leukoc. Biol.* **108**, 909–924. https://doi.org/10.1002/jlb.2mr0420-152r (2020).
43. Brown, P. J. et al. N-terminally truncated FOXP1 protein expression and alternate internal FOXP1 promoter usage in normal and malignant B cells. *Haematologica* **101**, 861–871. https://doi.org/10.3324/haematol.2016.142141 (2016).
44. Hoss, F. et al. Alternative splicing regulates stochastic NLRP3 activity. *Nat. Commun.* **10**, 3238. https://doi.org/10.1038/s41467-019-11076-1 (2019).
45. Kalam, H., Fontana, M. F. & Kumar, D. Alternate splicing of transcripts shape macrophage response to *Mycobacterium tuberculosis* infection. *PLoS Pathog.* **13**, e1006236. https://doi.org/10.1371/journal.ppat.1006236 (2017).
46. Mancl, M. E. et al. Two discrete promoters regulate the alternatively spliced human interferon regulatory factor-5 isoforms. Multiple isoforms with distinct cell type-specific expression, localization, regulation, and function. *J. Biol. Chem.* **280**, 21078–21090. https://doi.org/10.1074/jbc.M500543200 (2005).
47. Lambert, J. M., Ashi, M. O., Srour, N., Delpy, L. & Saulière, J. Mechanisms and regulation of Nonsense-Mediated mRNA decay and Nonsense-Associated altered splicing in lymphocytes. *Int. J. Mol. Sci.* **21**(4), 1335. https://doi.org/10.3390/ijms21041335 (2020).
48. Ullrich, S. & Guigó, R. Dynamic changes in intron retention are tightly associated with regulation of splicing factors and proliferative activity during B-cell development. *Nucleic Acids Res.* **48**, 1327–1340. https://doi.org/10.1093/nar/gkz1180 (2020).
49. Kay, R. R. Macropinocytosis Biology and mechanisms. *Cells Dev.* **168**, 203713. https://doi.org/10.1016/j.cdev.2021.203713 (2021).
50. Sundqvist, G., Figdor, D., Hänström, L., Sörlin, S. & Sandström, G. Phagocytosis and virulence of different strains of *Porphyromonas gingivalis*. *Scand. J. Dent. Res.* **99**, 117–129. https://doi.org/10.1111/j.1600-0722.1991.tb01874.x (1991).
51. de Pablo, P., Chapple, I. L., Buckley, C. D. & Dietrich, T. Periodontitis in systemic rheumatic diseases. *Nat. Rev. Rheumatol.* **5**, 218–224. https://doi.org/10.1038/nrrheum.2009.28 (2009).
52. Takamura, H., Yoshida, K., Okamura, H., Fujiwara, N. & Ozaki, K. Porphyromonas gingivalis attenuates the insulin-induced phosphorylation and translocation of forkhead box protein O1 in human hepatocytes. *Arch. Oral Biol.* **69**, 19–24. https://doi.org/10.1016/j.archoralbio.2016.05.010 (2016).
53. Ishikawa, M. et al. Oral *Porphyromonas gingivalis* translocates to the liver and regulates hepatic glycogen synthesis through the Akt/GSK-3β signaling pathway. *Biochim. Biophys. Acta* **1832**, 2035–2043. https://doi.org/10.1016/j.bbadis.2013.07.012 (2013).
54. Olsen, I., Singhrao, S. K. & Potempa, J. Citrullination as a plausible link to periodontitis, rheumatoid arthritis, atherosclerosis and Alzheimer's disease. *J. Oral Microbiol.* **10**, 1487742. https://doi.org/10.1080/20002297.2018.1487742 (2018).
55. Dominy, S. S. et al. Porphyromonas gingivalis in Alzheimer's disease brains: Evidence for disease causation and treatment with small-molecule inhibitors. *Sci. Adv.* **5**, eaau3333. https://doi.org/10.1126/sciadv.aau3333 (2019).
56. Tanai, A. & Okamura, H. The role of extracellular vesicles throughout normal pregnancy and in relation to oral bacteria. *J. Oral Biosci.* **63**, 14–22. https://doi.org/10.1016/j.job.2021.01.006 (2021).
57. Okamura, H. et al. Outer membrane vesicles of Porphyromonas gingivalis: Novel communication tool and strategy. *Jpn Dent. Sci. Rev.* **57**, 138–146. https://doi.org/10.1016/j.jdsr.2021.07.003 (2021).
58. Xie, H. Biogenesis and function of *Porphyromonas gingivalis* outer membrane vesicles. *Future Microbiol.* **10**, 1517–1527. https://doi.org/10.2217/fmb.15.63 (2015).
59. Lunar Silva, I. & Cascales, E. Molecular strategies underlying *Porphyromonas gingivalis* virulence. *J. Mol. Biol.* **433**, 166836. https://doi.org/10.1016/j.jmb.2021.166836 (2021).
60. Carlisle, M. D., Srikantha, R. N. & Brogden, K. A. Degradation of human alpha- and beta-defensins by culture supernatants of *Porphyromonas gingivalis* strain 381. *J. Innate Immun.* **1**, 118–122. https://doi.org/10.1159/000181015 (2009).
61. Wilensky, A., Tzach-Nahman, R., Potempa, J., Shapira, L. & Nussbaum, G. *Porphyromonas gingivalis* gingipains selectively reduce CD14 expression, leading to macrophage hyporesponsiveness to bacterial infection. *J. Innate Immun.* **7**, 127–135. https://doi.org/10.1159/000365970 (2015).
62. Patel, S. B. & Bellini, M. The assembly of a spliceosomal small nuclear ribonucleoprotein particle. *Nucleic Acids Res.* **36**, 6482–6493. https://doi.org/10.1093/nar/gkn658 (2008).
63. Saltzman, A. L., Pan, Q. & Blencowe, B. J. Regulation of alternative splicing by the core spliceosomal machinery. *Genes Dev.* **25**, 373–384. https://doi.org/10.1101/gad.2004811 (2011).
64. Nakagaki-Silva, E. E. et al. Identification of RBPMS as a mammalian smooth muscle master splicing regulator via proximity of its gene with super-enhancers. *Elife* **8**, e46327. https://doi.org/10.7554/eLife.46327 (2019).
65. Barnhart, M. D. et al. Phosphorylation of the smooth muscle master splicing regulator RBPMS regulates its splicing activity. *Nucleic Acids Res.* **50**, 11895–11915. https://doi.org/10.1093/nar/gkac1048 (2022).
66. Yang, Y. et al. Cell-type specific regulator RBPMS switches alternative splicing via higher-order oligomerization and heterotypic interactions with other splicing regulators. *Nucleic Acids Res.* **51**, 9961–9982. https://doi.org/10.1093/nar/gkad652 (2023).
67. Shi, Y. et al. Genetic analyses of proteolysis, hemoglobin binding, and hemagglutination of *Porphyromonas gingivalis*. Construction of mutants with a combination of RgpA, RgpB, Kgp, and HagA. *J. Biol. Chem.* **274**, 17955–17960. https://doi.org/10.1074/jbc.274.25.17955 (1999).
68. Abramson, J. et al. Accurate structure prediction of biomolecular interactions with alphafold 3. *Nature* **630**, 493–500. https://doi.org/10.1038/s41586-024-07487-w (2024).
69. Reva, B. A., Finkelstein, A. V. & Skolnick, J. What is the probability of a chance prediction of a protein structure with an Rmsd of 6 A? *Fold. Des.* **3**, 141–147. https://doi.org/10.1016/s1359-0278(98)00019-4 (1998).

Acknowledgements

The authors are grateful to Professor Mariko Naito and Assistant Professor Miko Shoji (Department of Molecular Microbiology and Immunology, Nagasaki University) for providing ΔKDP strains in the study.

Author contributions

Yilin Zheng: Conceptualization, Methodology, Investigation, Data curation, Visualization, Formal analysis, Resources, Writing- Original draft preparation. Ziyi Wang: Software, Conceptualization, Methodology, Data curation, Formal analysis, Visualization, Writing - Reviewing and Editing, Resources. Yao Weng: Formal analysis, Resources, Writing - Reviewing and Editing. Heriati Sitosari: Formal analysis, Visualization, Writing - Reviewing and Editing. Yuhan He: Formal analysis, Visualization, Writing - Reviewing and Editing. Xiu Zhang: Investigation, Visualization, Writing - Reviewing and Editing. Noriko Shiotsu: Resources. Yoko Fukuhara: Formal Analysis, Resources, Writing - Reviewing and Editing. Mika Ikegame: Project administration, Resources, Funding acquisition, Writing- Reviewing and Editing. Hirohiko Okamura: Methodology, Supervision, Project administration, Resources, Funding acquisition, Writing- Reviewing and Editing.

Funding

This study was funded by a Grant-in-Aid for Scientific Research from the Ministry of Education, Science, Sports, and Culture of Japan (23K18431, 22H03511, 21K19644, HO; 22H06790, MI).

Declarations

Competing interests

The authors declare no competing interests.

Additional information

Supplementary Information The online version contains supplementary material available at https://doi.org/10.1038/s41598-025-94954-7.

Correspondence and requests for materials should be addressed to H.O.

Reprints and permissions information is available at www.nature.com/reprints.

Publisher's note Springer Nature remains neutral with regard to jurisdictional claims in published maps and institutional affiliations.